Research Square

Preprints are preliminary reports that have not undergone peer review.
They should not be considered conclusive, used to inform clinical practice,
or referenced by the media as validated information.

Adhesion, Wettability, and In Vitro Cellular Response of Heat-Treated TiO_2 Nanotubes Produced by Fast Anodization

Bruno Cesar Nepomoceno Silveira
Pontifícia Universidade Católica do Paraná
Abhishek Bhattacharjee
Colorado State University
Ketul C. Popat
Colorado State University
Paulo Soares
pa.soares@pucpr.br

Pontifícia Universidade Católica do Paraná

Research Article

Keywords: TiO2 nanotubes, Ultrafast anodization, Dental implants, Wettability, Cell adhesion

Posted Date: September 10th, 2026

DOI: https://doi.org/10.21203/rs.3.rs-10883838/v1

License: This work is licensed under a Creative Commons Attribution 4.0 International License.
Read Full License

Additional Declarations: No competing interests reported.

Adhesion, Wettability, and In Vitro Cellular Response of Heat-Treated TiO_2 Nanotubes Produced by Fast Anodization

Bruno Cesar Nepomoceno da Silveira[1], Abhishek Bhattacharjee[2], Ketul C. Popat[3], Paulo Soares[1]

[1]Department of Mechanical Engineering, Polytechnic School, Pontifical Catholic University of Parana, Curitiba, PR, Brazil

[2]School of Advanced Materials Discovery, Colorado State University, Fort Collins, CO, USA

[3]School of Biomedical and Chemical Engineering, Colorado State University, Fort Collins, CO, USA

Abstract

The long-term performance of dental implants is strongly influenced by the physicochemical, morphological, and biological characteristics of their surfaces. In this study, a rapid anodization route was used to produce TiO_2 nanotube layers on commercially pure grade 4 titanium. Titanium sheets, discs, and machined dental implants were anodized at 140 V for 2 min in an electrolyte containing lactic acid, NH_4F, water, and ethylene glycol, followed by heat treatment at 530 °C for 1 h. Scanning electron microscopy revealed a continuous nanotubular layer with an approximate thickness of 6 μm and nanotube diameters of approximately 120 nm. X-ray diffraction indicated that the initially amorphous anodic oxide was converted into a crystalline layer containing predominantly anatase TiO_2 after heat treatment. The treated flat surfaces exhibited a water contact angle below the reliable measurement limit and reported as approximately 0°, whereas the untreated surfaces showed contact angles above 60°. Qualitative SEM assessment after scratch testing and implant insertion indicated reduced visible coating detachment after heat treatment under the tested mechanical conditions. In vitro biological assays using human adipose-derived stem cells, showed higher metabolic activity and cell numbers on the anodized surfaces than on untreated titanium, together with low LDH release and more extensive cell spreading. These findings indicate that rapid anodization followed by annealing can produce a highly wettable TiO_2 nanotube layer with favorable short-term in vitro cellular responses and qualitative resistance to coating detachment under the evaluated conditions. Further quantitative mechanical testing, osteogenic assays, long-term biological studies, and in vivo investigations are required to determine the potential of this surface treatment for improving osseointegration and supporting clinical translation.

Keywords

TiO_2 nanotubes; Ultrafast anodization; Dental implants; Wettability; Cell adhesion.

1 Introduction

Titanium and its alloys remain the primary materials for dental and orthopedic implants because of their mechanical strength, corrosion resistance, and biological compatibility [1]. Long-term implant success is closely related not only to the bulk composition but also to the micro- and nanoscale characteristics of the implant surface. Conventional surface treatments, such as blasting and acid etching, produce microrough surfaces that may improve bone anchorage; however, protein adsorption and early cellular interactions are also strongly influenced by nanoscale surface features. Consequently, titania nanotube arrays have been investigated as a potential strategy to modify titanium surfaces and support favorable early cellular responses.

Titanium dioxide nanotubes (TNTs) provide an ordered nanoscale topography whose diameter, length, spacing, wall thickness, crystallinity, and surface chemistry can be influenced by the anodization and post-treatment conditions [2–6]. These characteristics may affect protein adsorption and conformation, thereby influencing integrin-mediated cell adhesion and subsequent cellular behavior [5,6]. Previous studies have reported that TNT surfaces can modify cell adhesion, cytoskeletal organization, metabolic activity, and osteogenic-related responses [2–4,7]. However, these effects should not be attributed to nanotube diameter alone. The biological response depends on the combined influence of nanotube geometry, surface roughness, crystallinity, chemical composition, substrate, cell type, culture conditions, and experimental design.

Some studies have associated smaller nanotube diameters with improved early cell attachment and filopodia extension, whereas other studies have reported stronger osteogenic-related responses for larger nanotube architectures [2,7]. These findings suggest that nanotube dimensions may influence different aspects of cell behavior. Nevertheless, the reported diameter ranges should not be interpreted as universal thresholds because the results may vary according to the complete surface architecture and the biological conditions used in each study.

TNT surfaces have also been investigated in relation to platelet interactions, macrophage responses, angiogenic behavior, and osteogenic differentiation [7–11]. These studies provide a biological motivation for the development of nanostructured titanium surfaces. However, platelet activation, macrophage polarization, angiogenesis, osteogenic differentiation, mineralization, and in vivo osseointegration were not directly evaluated in the present study. The biological assessment performed here was limited to short-term in vitro responses of human adipose-derived stem cells, including metabolic activity, LDH release, cell adhesion, cell morphology, and cell number.

The formation of TiO_2 nanotubes during titanium anodization results from the dynamic interaction between oxide growth and oxide dissolution at the metal surface [12–14]. When titanium is polarized in a fluoride-containing electrolyte, the electric field promotes oxide formation at the metal/oxide interface, while fluoride-containing species contribute to the localized dissolution of TiO_2 at the oxide/electrolyte interface. When these processes are appropriately balanced, the initial compact oxide layer can develop into porous and subsequently organized nanotubular structures [12,15].

The applied voltage is one of the main parameters affecting TNT formation. It influences the electric field across the oxide and may affect the pore or nanotube diameter, although this relationship depends on the electrolyte, substrate, current response, and reactor configuration. Moderate voltages may favor uniform nanotube formation, whereas excessively high voltages can result in dielectric breakdown, local burning, or morphological irregularities [15,16]. Anodization time also affects oxide growth and nanotube length. Initially, the layer may grow rapidly, but the growth rate can decrease as the oxide becomes thicker and dissolution processes become more significant [16–18].

Electrolyte composition also plays an important role in nanotube formation. Fluoride concentration influences oxide dissolution, while water content, pH, solvent viscosity, and temperature affect the balance between oxide growth and dissolution [19–25]. Low fluoride concentrations may result in compact or weakly porous layers, whereas excessive fluoride concentrations may cause aggressive dissolution, wall thinning, or the formation of irregular structures [19,20]. Organic solvents such as ethylene glycol and glycerol can reduce the chemical aggressiveness of the electrolyte and may promote the formation of more uniform nanotube layers [19,21–23]. The substrate itself also affects nanotube development because crystallographic orientation, grain structure, alloy composition, and phase distribution can influence local electrochemical reactivity [26].

The formation of TNT layers is commonly reported for processing times ranging from several minutes to several hours, although the required time depends strongly on the applied voltage, current density, electrolyte composition, substrate, target nanotube dimensions, treatment area, and reactor configuration [16–18,27]. Therefore, a shorter anodization time alone does not establish that a process is industrially viable. Industrial application would also require evidence of reproducibility, process yield, treatment-area scalability, energy consumption, electrolyte stability, quality control, and batch-to-batch consistency.

Lactic acid-containing electrolytes have been investigated as a strategy for accelerating the formation of anodic TiO_2 nanotubes. Organic species may influence dissolution kinetics and allow nanotube growth under relatively high-voltage conditions [27]. So et al. reported the ultrafast growth of highly ordered anodic TiO_2 nanotubes using a lactic-acid-based electrolyte [27]. These findings indicate that rapid nanotube formation is possible under suitable electrochemical conditions. However, additional characterization is required to determine whether the resulting layer is sufficiently uniform, mechanically resistant, and biologically favorable when applied to dental implant geometries.

Heat treatment after anodization is commonly used to modify the crystallinity and physicochemical properties of TiO_2 nanotube layers [28–30]. Amorphous anodic TiO_2 can be converted into crystalline anatase, and rutile may also form depending on the temperature and treatment conditions. Annealing may additionally influence residual species, interfacial stresses, nanotube-wall consolidation, and coating adhesion [28–31]. These changes may affect wettability, mechanical integrity, and cell behavior. However, the biological response after heat treatment cannot be attributed exclusively to crystallinity because annealing may simultaneously alter nanotube morphology, surface chemistry, roughness, and adhesion.

Despite the biological interest in TNT surfaces, the combined evaluation of nanotube morphology, crystallinity, wettability, mechanical integrity, and short-term cellular response after ultrafast anodization on dental implant geometries remains limited. In particular, few studies have examined whether a nanotubular layer produced within a short processing time can be formed on threaded dental implants and remain attached during a placement-like mechanical procedure. This knowledge gap is relevant because coating integrity during implantation may influence the preservation of the intended surface characteristics.

In the present work, preliminary anodization screening was performed using voltages ranging from 80 to 180 V and anodization times ranging from 1 to 10 min. The condition of 140 V for 2 min was selected because it produced a continuous and visually uniform nanotubular layer under the experimental conditions used. Because the screening procedure was not designed as a statistically validated optimization study, the selected condition is considered a preliminary process window rather than an optimized condition in a formal statistical sense. The exact number of tested specimens and the criteria used to classify a coating as successful should be reported to improve the reproducibility of this selection procedure.

The objective of this study was to evaluate whether rapid anodization could produce a continuous TiO_2 nanotube layer on commercially pure grade 4 titanium sheets, discs, and machined dental implants. The study specifically aimed to characterize the nanotube morphology and crystalline phases; assess wettability on flat and implant-like geometries; evaluate the qualitative integrity of the coating after scratch testing and implant insertion; and investigate the short-term in vitro response of human adipose-derived stem cells through metabolic activity, LDH release, cell adhesion, cell morphology, and cell number. These results were used to assess the surface and preliminary biological characteristics of the proposed rapid anodization route, without directly establishing osteogenic differentiation, osseointegration, industrial scalability, or clinical performance.

2 Materials and methods

2.1 Samples preparation

Three different types of commercially pure grade 4 titanium samples were subjected to anodization to produce a layer of TiO_2 nanotubes (Figure 1):

- Type 1: Titanium sheets measuring 60 × 5 × 2 mm (Acnis do Brazil).
- Type 2: Titanium discs with a diameter of 6 x 1 mm (Ti sheets cut using wire-EDM).
- Type 3: Titanium dental implants (GM Helix, Neodent, Curitiba-Brazil) featuring a machined surface (i.e., without any previous surface treatment).

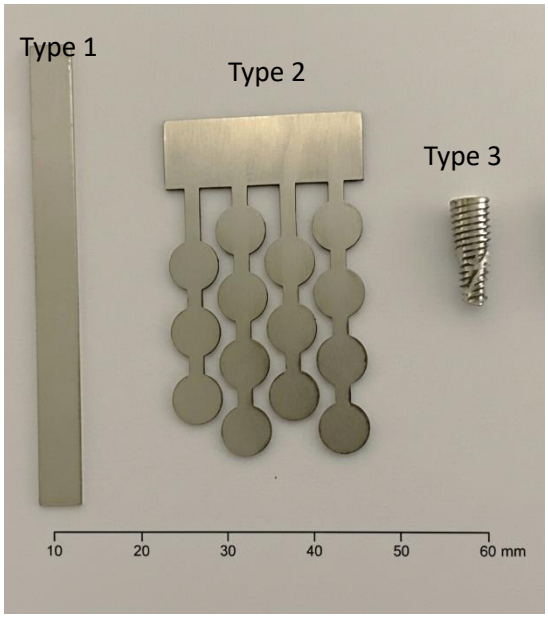


Figure 1. Types of commercially pure grade 4 titanium samples used in this work.

All sample types, sheets, discs, and implants, underwent identical surface preparation prior to anodization. The preparation consisted of a three-step ultrasonic cleaning procedure, with each step lasting 5 minutes, sequentially using acetone, isopropyl alcohol, and deionized water. Following, the samples were air dried before anodization.

Several anodization conditions were initially evaluated to identify a fast-route parameter capable of producing a uniform and well-defined TiO_2 nanotubular layer. Preliminary screening tests were performed using applied voltages ranging from 80 to 180 V and anodization times ranging from 1 to 10 min. These tests were conducted to identify a condition capable of producing a continuous and visually uniform nanotubular layer on the titanium substrates. Lower voltages (≤120 V) or short times (≤1 min) typically resulted in incomplete or irregular nanotube formation, while higher voltages (>150 V) or extended times (>5 min) frequently led to dielectric breakdown, oxide burning, or heterogeneous surface morphology. Intermediate conditions (e.g., 130 V for 2 min) produced more consistent nanotube initiation but still showed local defects and non-uniform tube distribution. Based on the qualitative observation of coating continuity and surface uniformity, the condition of 140 V for 2 min was selected for the subsequent experiments. This parameter provided the optimal balance between rapid oxide growth, morphological uniformity, and process stability, and was therefore selected as the single anodization condition reported in the manuscript.

Anodization was performed in a two-electrode electrochemical cell using the titanium sample as the anode and a platinum foil as the counter-electrode. The distance between the counter-electrode and the titanium sample was maintained at approximately 20 mm. The electrolyte temperature was maintained at 25 °C before anodization. Anodization was conducted under constant voltage at 140 V for 2 min. The electrolyte contained 1.5 M lactic acid, 0.1 M NH_4F,

5 wt.% water, and 1 L of ethylene glycol. Figure 2 presents a schematic illustration of the anodization setup used in this study.

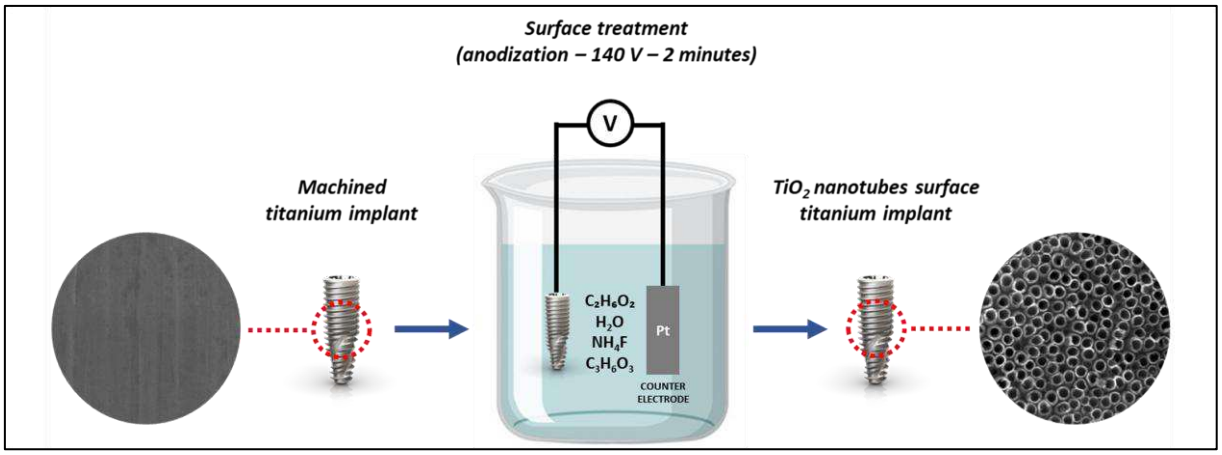


Figure 2. Schematic representation of the anodization setup and the formation mechanism of TiO_2 nanotubes in a fluoride-containing electrolyte.

All anodized samples were subjected to a heat treatment at 530 °C for 1 h, using a controlled heating rate of 5 °C·min^{-1} in an electric furnace (EDG 3000, with ±1°C control), in order to promote crystallization of the anodic oxide layer and improve its adhesion to the metallic substrate. This temperature was selected based on previous studies reporting that heat treatment in this range promotes the crystallization of anodic TiO_2 and can improve the integrity and adhesion of TiO_2 nanotube layers [29,32]

2.2 Surface characterization

2.2.1 Scanning Electron Microscopy (SEM)

The morphology of the anodized and heat-treated surfaces was analyzed using SEM (Vega 3 – Tescan). Micrographs were acquired at different magnifications to assess the homogeneity of the oxide layer, the presence of nanotube structures, and any morphological changes resulting from heat treatment or mechanical testing (scratch and insertion). For implant samples, SEM was also used to compare the surface before and after insertion into polyurethane, enabling evaluation of coating integrity.

2.2.2 Glancing Angle X-ray Diffraction (GA-XRD)

XRD analyses were performed to determine the crystalline phases present after heat treatment at 530 °C. Diffractograms were collected using Cu-Kα radiation, 2θ range of 20 to 80°, speed 2°/min, incident angle of 5° (Shimadzu, XRD-7000 Maxima). Peaks were indexed to identify the crystallographic structure of the TiO_2 film using the software Match! and the ICDD-PDF2 database.

2.2.3 Wettability

Wettability was evaluated using two complementary methods to account for the different geometries of the samples. For flat titanium discs, the static contact angle was measured using the sessile drop method. A 2 µL droplet of deionized water was gently deposited on the sample

surface, and images were captured immediately after deposition to avoid evaporation-induced variations, using a goniometer (Krüss, EasyDrop DSA20E) Contact angles were calculated using a standard goniometric algorithm based on the Young–Laplace fitting procedure. Each surface was measured at three distinct locations, and the reported values represent the mean ± standard deviation.

For cylindrical implant-like samples, the static sessile drop method could not be applied reliably due to curvature effects. Therefore, dynamic contact angle measurements were performed using the Wilhelmy plate method (Krüss, K100C). Samples were vertically immersed and withdrawn from water at a constant speed while the wetting force was recorded continuously. The advancing and receding contact angles were obtained from the linear region of the force–position curve, considering the known perimeter of each sample and the surface tension of water. Buoyancy corrections were applied following standard Wilhelmy theory. The contact angle was computed using:

$$\theta = cos^{-1}\left(\frac{F_w}{L\gamma_{lv}}\right) \quad (1)$$

Where the contact angle can be determined by knowing the force (F_w) at the 0 position of advancing, L is the perimeter of immersed sample (wetted length), γ_{lv} is the liquid-vapor surface tension [33]. All measurements were performed at room temperature (~23 °C) under controlled humidity.

The combined use of sessile drop and Wilhelmy methods ensures accurate evaluation of wettability on both flat and cylindrical surfaces, avoiding geometric artifacts that would compromise comparability.

2.3 Adhesion Evaluation

Adhesion of the anodic TiO_2 nanotube (TNT) layer to the Ti Grade 4 substrate was assessed qualitatively using two complementary approaches selected according to sample geometry: (i) instrumented scratch testing for flat specimens (Type 1) and (ii) an insertion test for dental implants (Type 3) to reproduce the mechanical severity associated with clinical placement.

For the scratch test, adhesion was evaluated using a nanoindenter equipped with a spherical diamond tip (Zwick Roell, ZHN Nanoindenter). A progressive normal load from 0 to 500 mN was applied over a 350 μm scratch length under controlled penetration depth. After testing, scratched tracks were examined by SEM (Zeiss, Gemini) to identify failure features indicative of interfacial weakness. In this framework, coatings exhibiting edge-lift and interfacial delamination adjacent to the track were classified as poorly adhered, whereas coatings showing material removal largely confined to the scratch groove were classified as well adhered.

For the insertion test, implant adhesion was evaluated under conditions intended to mimic placement into low-density bone. Dental implants were inserted into 10 PCF polyurethane blocks (Nacional Ossos), which are commonly used as a surrogate for poor-quality bone where

surface treatments are expected to be most relevant for secondary stability. Osteotomy preparation was performed following a drilling sequence analogous to clinical bone-bed preparation. Implants were inserted using an electromechanical universal testing machine (Walter + Bai, LFM-L) at a constant rotational speed of 30 rpm. The integrity of the TNT layer was then assessed by comparative SEM of the surface before and after insertion, with attention to detachment, abrasion, or gross damage to the nanotube layer.

2.4 Biocompatibility of anodized samples

The biological characterization of the anodized surfaces was performed using human adipose-derived stem cells (ADSCs) to evaluate cytotoxicity, viability, adhesion, proliferation, and morphology. Before cell seeding, all samples were sterilized by immersion in 70% ethanol followed by drying under aseptic conditions.

The ADSCs used in this study were donated by Dr. Kimberly Cox-York (Colorado State University), with isolation approved by the institution's IRB. Cells were cultured at 37 °C in a growth medium composed of 90% MEM Alpha, 9% fetal bovine serum, and 1% penicillin–streptomycin. After sterilization, ADSCs were seeded on each surface at a density of 20,000 cells per well.

Cytotoxicity and viability were assessed using alamarBlue™ and lactate dehydrogenase (LDH) assays. ADSCs at passage 5 were seeded on sterilized samples at a density of 20,000 cells per well and incubated at 37 °C. Cell viability was quantified after 1, 4, and 7 days of culture using the alamarBlue™ Assay Reagent (Promega). At each time point, samples were incubated for 4 h at 37 °C in fresh α-MEM supplemented with 10% alamarBlue™. The reagent, initially blue in its oxidized form, is reduced to a red fluorescent product by metabolically active cells. After incubation, the optical density was measured at and 600 nm using a microplate spectrophotometer (FLUO-star Omega, BMG Labtech), and the percentage reduction of alamarBlue™ was calculated following the manufacturer's instructions.

Cytotoxicity was evaluated after 24 h of culture using the LDH Assay Kit (Cayman Chemical). In addition to the experimental groups, ten control wells containing only ADSCs in α-MEM were included: five served as negative controls, and five were treated with 10% Triton-X to induce complete cell lysis for the positive control. After 24 h, 100 µL of culture medium from each well was transferred to a 96-well plate, mixed with 100 µL of LDH working solution, and incubated for 30 min on an orbital shaker. Absorbance was then measured at 490 nm (BMG Labtech) to determine LDH release. Cytotoxicity was calculated relative to spontaneous (untreated cells) and maximum (Triton-X lysed cells) LDH release, following the manufacturer's analytical formula.

Cell adhesion, proliferation, and morphology were evaluated at multiple time points using fluorescence microscopy. After 4 and 7 days of culture, samples were washed with PBS to remove non-adherent cells and fixed in 3.7% formaldehyde for 15 min. The cells were permeabilized with 1% Triton X-100, and their actin cytoskeleton was stained with rhodamine-phalloidin, followed by DAPI staining for nuclei. After rinsing with PBS,

fluorescence images were acquired and analyzed to quantify the number of adherent cells and assess proliferation over time.

Morphological characterization of ADSCs on the surfaces was performed by SEM at selected time points. After 1, 4, and 7 days of culture, samples were washed with PBS and fixed in a solution containing 3% glutaraldehyde, 0.1 M sodium cacodylate, and 0.1 M sucrose for 45 min. The samples were then rinsed in buffer without glutaraldehyde and dehydrated through a graded ethanol series (35%, 50%, 70%, and 100%, 10 min each). Following dehydration, the surfaces were incubated in dexamethyldisilazane for 10 min, air-dried, and sputter-coated with a gold layer. SEM imaging was subsequently performed to evaluate cell spreading, anchorage, and interactions with the underlying surface topography (Jeol JSM-6500F).

2.5 Statistical analysis

For SEM-based morphology, at least five images were acquired per group. Contact-angle and adhesion measurements used three samples per condition. For adhesion and proliferation studies, a minimum of nine fluorescence images and five SEM images were analyzed per group. Cytotoxicity (LDH) and metabolic activity (alamarBlue^{TM}) were accessed from 3 samples for each group. Statistical differences were assessed using one-way ANOVA and Student's T-test, with a significance level of (***) $p < 0.001$.

3 Results and Discussion

3.1 Morphology (SEM)

SEM observations of flat surfaces anodized at 140 V for 2 min (Figure 3A) show a continuous and morphologically homogeneous TiO_2 nanotubular layer covering the Ti Grade 4 substrate. The surface exhibits the characteristic nanotubular/nanoporous architecture expected for anodic titania formed in fluoride-containing electrolytes under self-organized growth conditions.

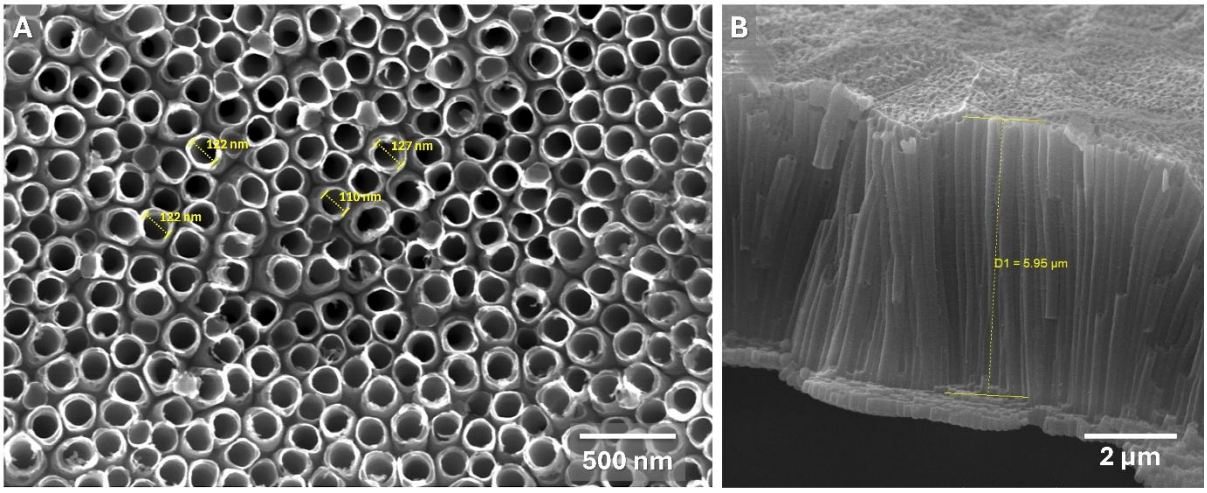


Figure 3. SEM images of (A) flat surfaces anodized at 140 V for 2 min showing homogeneous nanotube arrays and (B) cross-sectional view highlighting average nanotube length and diameter.

When the same anodization parameters were applied to cylindrical implants with a machined surface, SEM images indicate high morphological similarity to the nanotubular layer formed on flat samples. This result demonstrates that the proposed fast-route processing window is capable of generating nanotubular TiO_2 on non-planar geometries, provided that electrolyte access and electrical field distribution remain adequate along the implant surface.

Cross-sectional SEM of anodized specimens (Figure 3B) shows that the treatment produced an oxide layer with an approximate thickness of ~6 μm. Based on the provided description of the same cross-section, the nanotubes exhibit an approximate diameter of ~120 nm.

Nogueira et al. [34]reported TiO_2 nanotubes with ~130 nm diameter and ~5 μm length after anodization at 60 V for 45 min in a glycerol-based electrolyte containing 25 vol.% water and 0.25 M NH_4F. Under the present fast-route condition (140 V for 2 min, i.e., substantially shorter processing time), the nanotube dimensions described above (~120 nm diameter and ~6 μm layer thickness/length scale) are of comparable order, supporting the effectiveness of the accelerated route in achieving literature-consistent morphologies.

3.2 Crystallinity (XRD)

XRD patterns acquired from flat discs anodized at 140 V for 2 min were compared before and after heat treatment (Figure 4). For as-anodized condition (no heat treatment), diffractograms show Ti substrate peaks, indicating that the anodically formed TiO_2 nanotubes are predominantly amorphous. After heat treatment, the oxide layer exhibits clear crystallinity, with peaks assigned to anatase and rutile, with anatase predominance. Overall, the microstructural results demonstrate that the fast-route anodization reliably produces a nanotubular TiO_2 layer, with micrometer-scale thickness achieved in minutes, and with crystallinity tunable by post-anodization annealing.

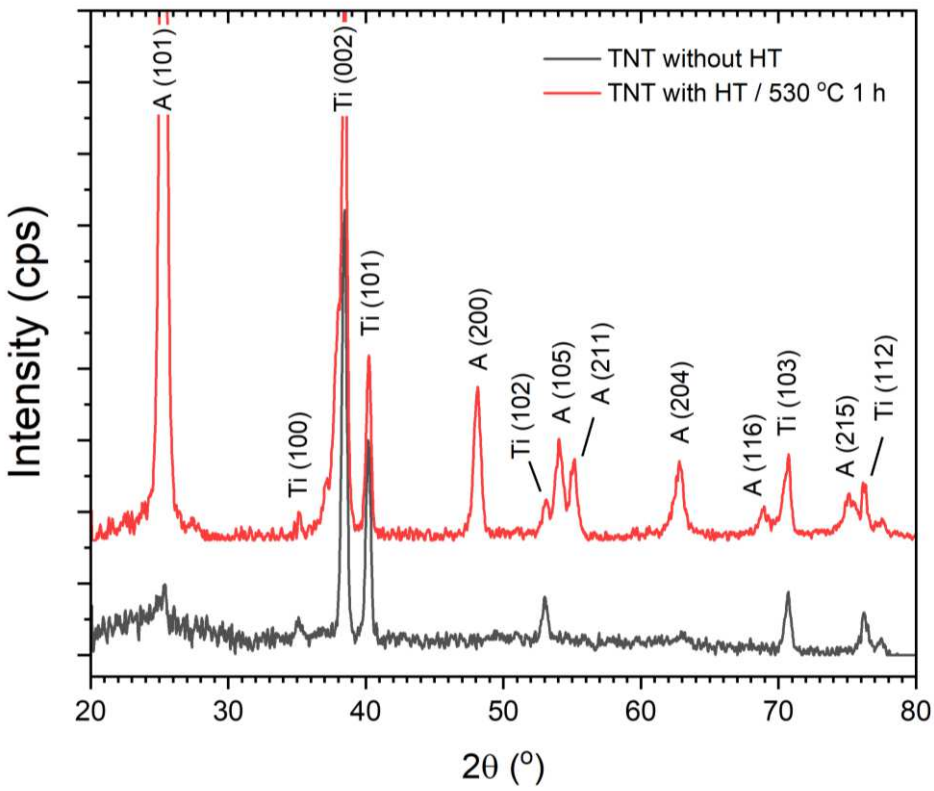


Figure 4. X-ray diffraction patterns of titanium samples anodized at 140 V for 2 min, recorded in the as-anodized condition and after heat treatment at 530 °C for 1 h, showing the transition from amorphous to anatase TiO_2.

3.3 Wettability

Figure 5 shows the water droplet on the flat surfaces, evaluated using the sessile drop method.

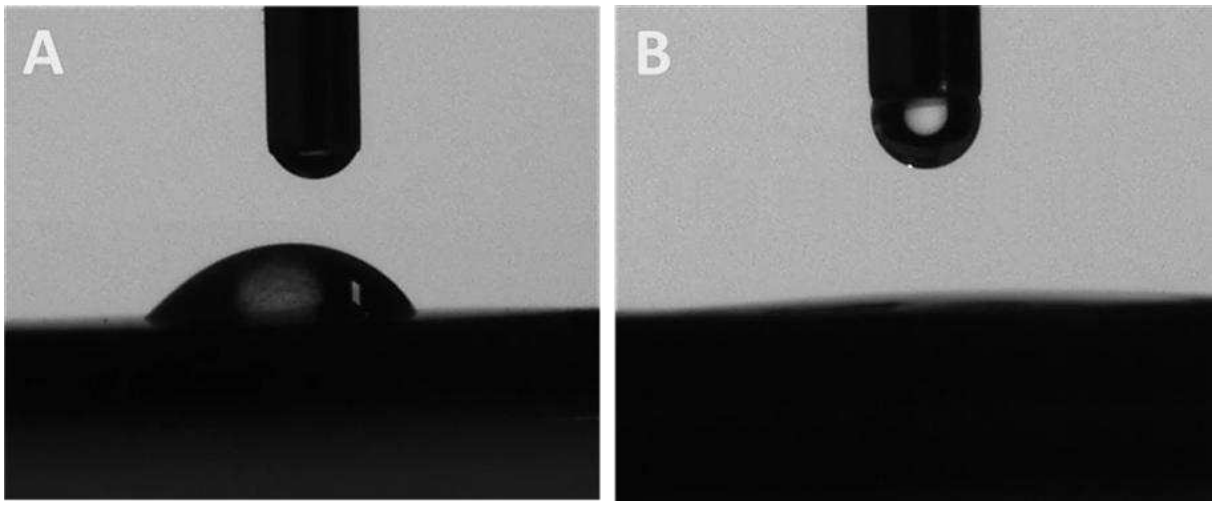


Figure 5. Sessile drop test on flat surfaces showing water contact angle for (A) untreated titanium and (B) anodized and heat-treated surfaces, demonstrating the transition to superhydrophilic behavior.

The untreated titanium surfaces exhibited hydrophilic behavior. Flat non-treated discs displayed contact angles exceeding 60°, consistent with the native TiO_2 passive film typically present on polished titanium surfaces.

In contrast, the anodized samples demonstrated superhydrophilic behavior, with a measured contact angle of ~ 0° on flat samples. The water droplet spread instantaneously across the nanotubular surface, preventing the formation of a measurable angle. This behavior was visually evident from the immediate disappearance of the droplet profile upon deposition.

The dynamic contact angle measured on anodized dental implants indicates that the contact angle for untreated and anodized samples was > 90º and 0º, respectively (Figure 6). Figure 6 shows the force in relation to advancing position of the implant into the saline solution.

Knowing the force at the zero point of advancing (obtained by linear fit), the samples perimeter (12.56 mm), and the surface tension of the saline solution (72.4 mN), it is possible to calculate the advancing contact angle, using Equation 1. For the sample to be considered superhydrophilic, the calculated contact angle must be ≤ 10º. Furthermore, when the calculation results in cos θ > 1, the contact angle is considered 0º, indicating superhydrophilicity.

For the machined implants, the cos θ < 1, with a contact angle of 90.4º, indicating a hydrophobic surface. On the other hand, for the anodized implant, as the cos θ > 1, the contact angle is considered 0º, indicating superhydrophilicity. Besides that, the surface obtained from the present work demonstrates better wettability than surfaces produced by a similar method found in the literature [34], with 0º (superhydrophilic) contact angle against contact angles varying between 20° and 65° (hydrophilic).

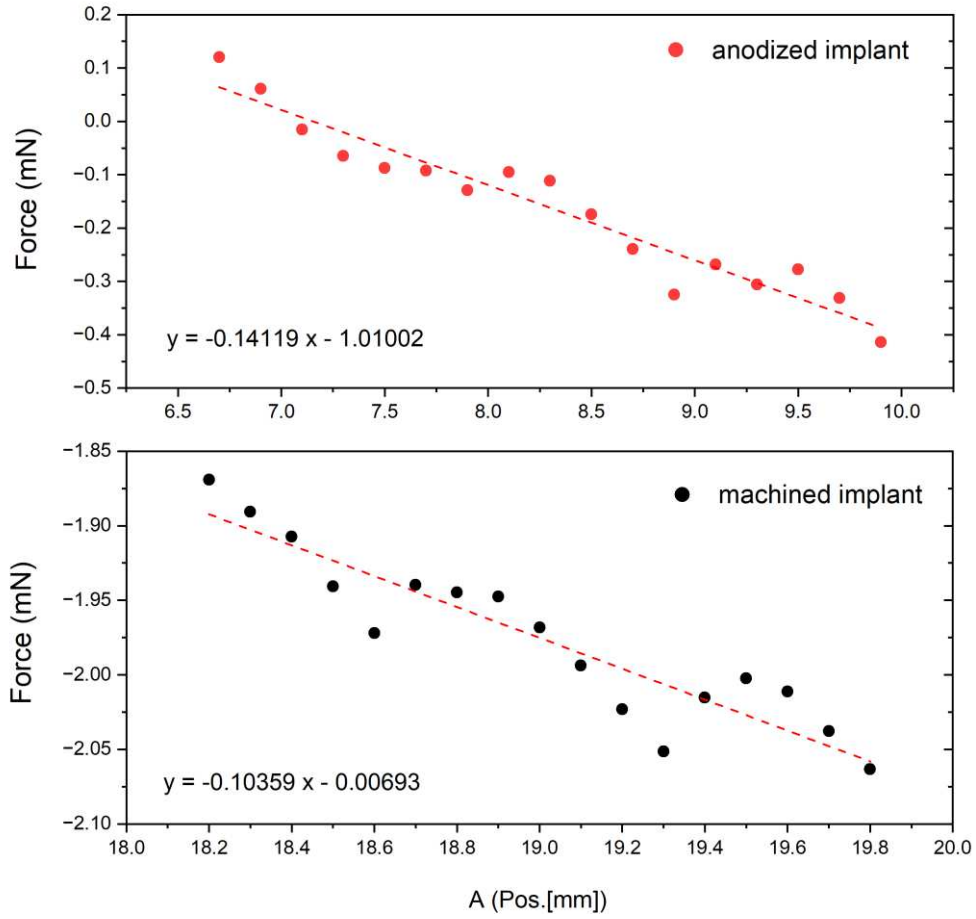


Figure 6. Force-to-position obtained from the advancing dynamic contact angle test with samples with and without anodization.

The transition from hydrophilic to superhydrophilic behavior after anodization is directly attributable to the formation of the TiO_2 nanotube (TNT) layer. The nanotubular morphology increases the effective surface area and capillary forces, enabling rapid spreading of water along the tube walls. This effect is well-established in the literature and is consistent with classical Wenzel and Cassie–Baxter wetting models, in which surface roughness amplifies the intrinsic wetting behavior of the underlying material.

After heat treatment, the TNT surface is primarily composed of anatase. Anatase is known to enhance hydrophilicity through increased density of surface hydroxyl groups and photocatalytically active sites, facilitating hydrogen bonding with water molecules [35]. This synergy between nanotopography and crystalline phase composition explains the superhydrophilic response observed. Moreover, superhydrophilicity has important implications for biological performance. Rapid protein adsorption, improved serum infiltration, and enhanced initial cell attachment are all promoted by high-energy hydrophilic surfaces [33,36]. These mechanisms directly align with the improved ADSC adhesion and proliferation shown in the biological assays.

The increase in wettability observed after anodization is consistent with classical reports on TiO_2 nanotube (TNT) surfaces, where hydrophilicity is enhanced through a combination of nanostructural geometry, surface chemistry, and crystallinity. Early work by Gong et al. [37] and Balaur et al. [38] demonstrated that vertically aligned nanotubular architectures drastically lower the water contact angle due to the formation of continuous capillary pathways that facilitate spontaneous water infiltration. This effect is particularly strong in nanotubes with open, well-defined morphologies, as produced in this study, which promote rapid spreading through a combination of increased surface area and capillary suction.

From a theoretical standpoint, the wetting behavior of TNT layers follows the Wenzel regime, wherein surface roughness amplifies the material's intrinsic wetting character. TiO_2 inherently exhibits moderate hydrophilicity in its hydroxylated state; however, after nanotube formation, the increased roughness factor magnifies this property, resulting in near-zero contact angles. Several studies, including those by Shin et al. [39], confirm that the transition to superhydrophilicity is typical in nanotube layers with diameters in the 20-120 nm range, as the roughness scaling promotes full wetting rather than composite wetting states.

The crystalline phase also plays a central role. Heat-treated TNT layers predominantly containing anatase exhibit higher wettability than amorphous films. Wang et al. [40] showed that anatase promotes enhanced surface hydroxylation and carries a higher density of oxygen vacancies and Ti^{3+} sites, features that increase water adsorption affinity. Our GA-XRD results confirm the formation of anatase during annealing, which explains the stability of the superhydrophilic state even after water exposure and mechanical handling.

Dynamic measurements using the Wilhelmy method further substantiate the high-energy wetting characteristics of TNTs. Advancing contact angles approaching zero suggest a surface with negligible contact angle hysteresis, indicative of uniform wetting across the entire surface rather than localized capillary trapping. Comparable behavior has been reported by Liu et al. [41], who attribute low hysteresis on TNT surfaces to the regularity of the nanotube array and its ability to maintain a continuous water front.

Importantly, the superhydrophilic nature of TNT surfaces is strongly correlated with improved biological interactions. Damodaran et al. [42] demonstrated that hydrophilic TiO_2 nanotube coatings accelerate protein adsorption kinetics, modulate the conformation of fibronectin and vitronectin, and increase initial cellular adhesion strength. The rapid wetting observed in our samples aligns with these findings and provides a mechanistic foundation for the enhanced ADSC adhesion and proliferation reported in the biological assays. The literature consistently shows that superhydrophilicity improves the early biological response by facilitating protein-mediated cell recruitment and spreading, ultimately contributing to enhanced osseointegration.

3.4 Adhesion

Figure 7 compares SEM observations after scratch testing for TNT layers produced by fast-route anodization with and without post-anodization heat treatment. The as-anodized condition (no heat treatment) exhibits detachment around the scratch track, indicating that fracture

propagated beyond the groove into the coating/substrate interface and promoted local delamination. In contrast, after heat treatment at 530 °C for 1 h, scratch damage is largely restricted to the track itself, with no evidence of extensive edge delamination, demonstrating a marked improvement in mechanical integrity and interfacial adhesion.

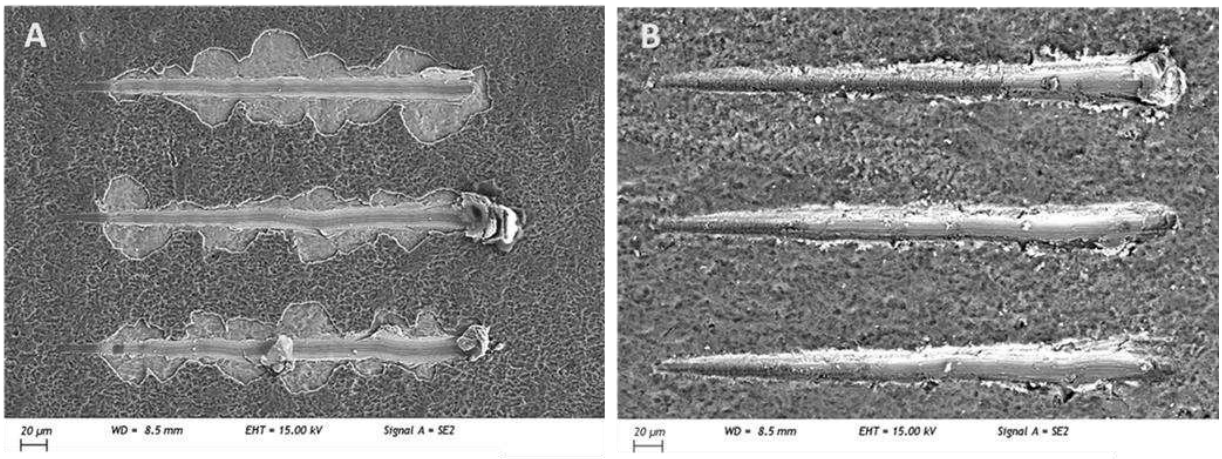


Figure 7. SEM images of TNT layers after instrumented scratch testing, comparing coatings produced by fast-route anodization (A) without and (B) with post-anodization heat treatment.

These findings are reinforced by the insertion test (Figure 8), which imposes a mechanically aggressive, clinically relevant combination of frictional shear and compressive contact during placement into a polyurethane block. The TNT-coated implant without heat treatment shows local coating detachment after insertion, whereas the heat-treated implant retains an intact TNT layer in the examined regions, indicating that annealing is critical to prevent mechanically driven spallation during insertion.

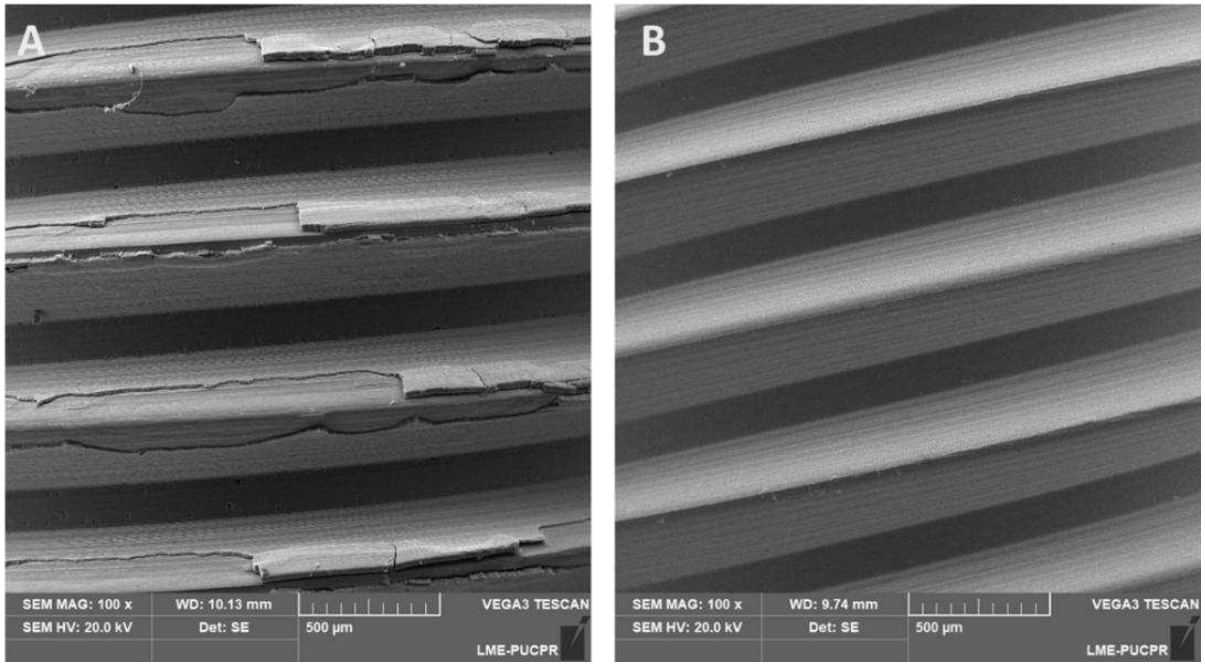


Figure 8. SEM images of the medial region of threaded implants after insertion into polyurethane foam, comparing nanotube integrity (A) without heat treatment and (B) after heat treatment.

The improved adhesion after annealing is consistent with the role of heat treatment in TNT systems, where thermal exposure promotes (i) oxide crystallization (anatase/rutile), (ii) structural consolidation/densification of tube walls, and (iii) stress relaxation and stabilization of the oxide/substrate interface. In fluoride-containing electrolytes, annealing can also stabilize the nanotube layer by reducing the detrimental effect of residual fluorinated species at or near the interface, thereby decreasing the likelihood of interfacial failure under shear. Importantly, the insertion test result demonstrates that the fast-route TNT layer can withstand a placement-like mechanical event only when an appropriate post-treatment is used, which directly supports the translational relevance of the proposed rapid anodization route.

The trend observed here agrees with prior work indicating that annealing near 530 °C provides a significant improvement in TNT-layer adhesion [31], and supports the selection of this heat-treatment condition as a practical balance between improving adhesion and avoiding thermal degradation of the nanotubular architecture.

Coating integrity during implant insertion is clinically critical because the placement event imposes high local contact stresses and frictional shear at the thread–bone interface, which can trigger partial detachment of poorly adherent anodic layers [43]. Any coating loss at this stage may generate oxide debris and leave regions of exposed substrate or mechanically smeared oxide, thereby altering the intended nanotopography and surface chemistry that govern initial protein adsorption, blood–implant interactions, and early cell attachment. Such insertion-induced surface disruption can therefore compromise the very early biological events that underpin secondary stability and osseointegration [44,45]. Our results show that the heat-treated TNT layer markedly mitigated this failure mode: SEM comparisons before and after insertion showed that annealed samples retained an intact nanotubular surface with no evidence of gross delamination, whereas non-heat-treated surfaces exhibited local detachment after placement.

3.5 Biocompatibility of anodized samples

ADSCs cultured on the anodized surfaces exhibited significantly higher metabolic activity at all time points compared to untreated titanium (Figure 9A). The increase was most pronounced at day 7, indicating sustained and progressive enhancement of cell viability on the nanotubular surface. These results align with previous reports showing that TiO_2 nanotubes, particularly those in the anatase phase, promote enhanced protein adsorption and integrin-mediated signaling, thereby stimulating cell proliferation [30].

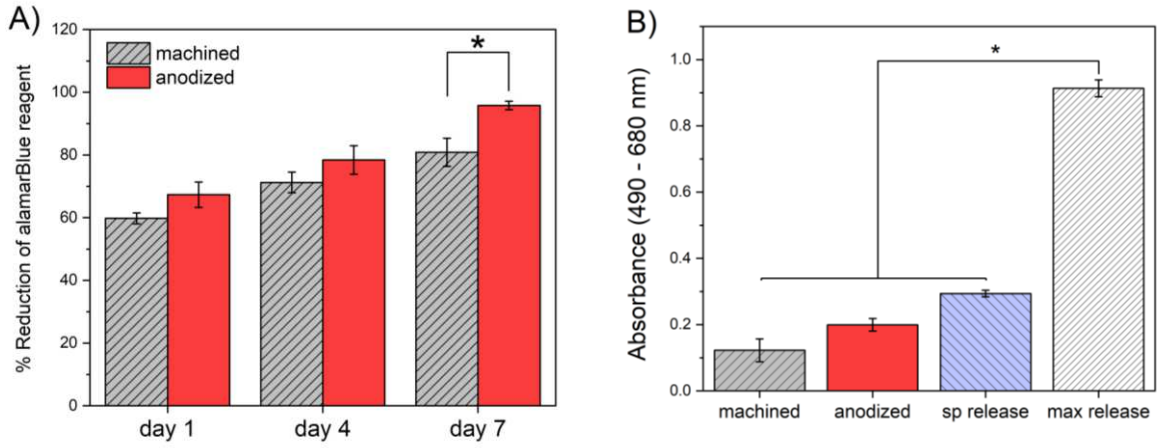


Figure 9. (A) Metabolic activity of ADSCs cultured on untreated and anodized surfaces after 1, 4, and 7 days (alamarBlue™ assay). (B) LDH release demonstrating negligible cytotoxicity for all groups. Significance: $p < 0.001$.

LDH release (Figure 9B) remained comparably low for both anodized and machined samples throughout the experiment, demonstrating that the fast-route anodization process and the subsequent heat treatment did not introduce cytotoxic residues or surface instabilities. This finding is consistent with the superhydrophilic nature of the anodized surface, which often reduces localized pH variations and ionic imbalance, mitigating potential cytotoxic effects.

SEM images revealed that ADSCs cultured on the anodized samples developed more extensive filopodia and exhibited greater cell spreading compared to controls (untreated) (Figure 10). The cells demonstrated well-defined actin networks and intimate contact with the nanotube openings, suggesting favorable nano-cell interactions. Fluorescence images corroborated these observations, showing denser and more uniform cellular coverage on treated surfaces over time.

These morphological characteristics indicate that the high surface energy and nanotube architecture promote early cell adhesion, a finding well documented in the literature but now validated for a fast, industrially viable anodization process.

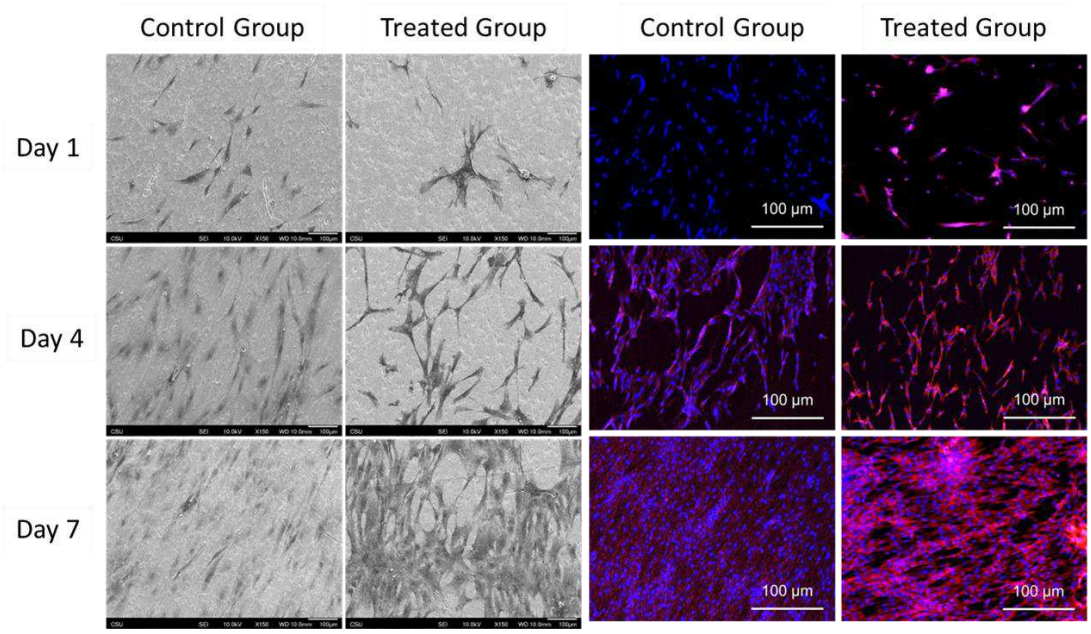


Figure 10. SEM and fluorescence microscopy images showing cellular morphology, spreading, and adhesion of ADSCs on machined control surfaces and anodized surfaces at different time points

Quantification of nuclei showed that cell numbers on anodized surfaces increased moderately from day 1 to day 4 (about 98%), but a much larger increase occurred between day 4 and day 7, reaching approximately 740% (Figure 11). In contrast, untreated titanium followed a different pattern: proliferation rose by about 146% from day 1 to day 4, but the subsequent increase from day 4 to day 7 was smaller (around 137%), indicating an earlier plateau. This behavior suggests that the nanotube topography not only supports but actively promotes prolonged proliferative activity. The enhanced proliferation is likely linked to (i) increased protein adsorption due to superhydrophilicity, (ii) favorable nanometric cues that guide cytoskeletal organization, and (iii) the predominance of the anatase crystalline phase after heat treatment, which has been previously correlated with positive cellular responses.

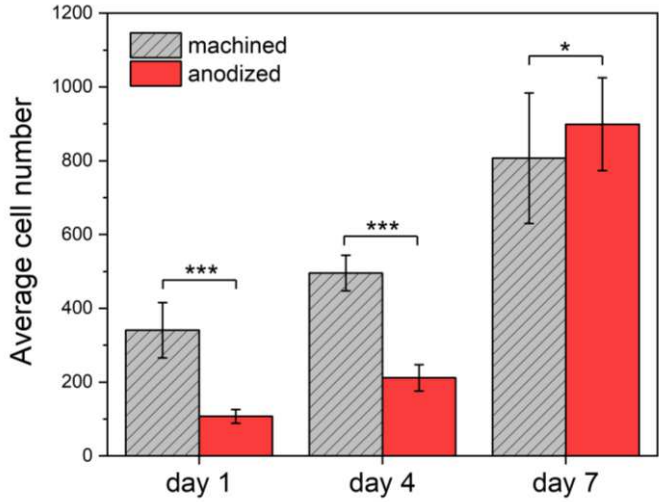


Figure 11. Quantification of ADSC proliferation on machined and anodized surfaces after 1, 4, and 7 days (DAPI-stained nuclei). Error bars represent mean ± SD. Significance levels: ***$p < 0.001$, *$p < 0.05$.

The biological results indicate that the fast-route anodization process produces a TiO_2 nanotube surface capable of supporting strong early cellular responses. The marked increases in metabolic activity and proliferation, together with the absence of cytotoxic effects, demonstrate that the resulting nanotube layer is highly compatible with ADSCs and creates a favorable microenvironment to early stages of osseointegration

These biological outcomes become even more meaningful when interpreted in light of the surface characterization data. The superhydrophilic nature of the treated samples, evidenced by a contact angle close to 0°, promotes rapid protein adsorption and, consequently, more efficient early cell attachment. At the same time, then nanotubular architecture provides nanoscale topographic cues that correspond closely to the dimensions at which integrin-mediated adhesion occurs, facilitating cell spreading and cytoskeletal organization. The predominance of the anatase crystalline phase further contributes to the positive response, as this phase is widely associated with the activation of osteogenic pathways in stem cells.

Complementing these biological advantages, the improved adhesion of the nanotube layer, confirmed through scratch and insertion tests, ensures that the surface modification remains mechanically stable, an essential requirement for load-bearing dental implant applications.

Taken together, these factors indicate that the enhanced biocompatibility observed in this study results from a synergistic combination of morphological, physicochemical, and mechanical improvements produced by the fast anodization process followed by annealing treatment.

4 Conclusions

The present study demonstrates that the fast-route anodization process, combined with a subsequent heat treatment, is an effective and reliable method for producing TiO_2 nanotube coatings with properties that directly support enhanced biological performance. The rapid anodization step, performed at high voltage for only two minutes, yielded a uniform nanotubular layer with well-defined morphology, while the heat treatment at 530 °C substantially improved its adhesion to titanium substrates. This combination ensured a mechanically stable surface capable of withstanding forces relevant to dental implant insertion and early functional loading.

Surface characterization revealed additional features that contribute to the improved biological response. The treated samples exhibited superhydrophilicity, a condition known to favor rapid protein adsorption and promote early cell anchorage. Crystallographic analysis confirmed the transition from an amorphous oxide to a predominantly anatase structure after heat treatment, a transformation associated with favorable interactions with stem cells and the initiation of osteogenic pathways. Together, these physicochemical attributes created a surface microenvironment highly conducive to cellular activity.

The biological assays reinforced these findings. ADSCs cultured on the treated surfaces showed consistently higher metabolic activity, robust adhesion marked by extensive filopodia, and progressive proliferation over time, with no indication of cytotoxic effects. This cellular behavior reflects the synergistic influence of the nanotube morphology, crystalline phase, and hydrophilic characteristics of the treated surfaces. The improved mechanical integrity of the nanotube layer ensures that these biological advantages are preserved throughout handling and implantation, addressing a critical requirement for clinical translation.

We can conclude that the fast anodization route, when paired with heat treatment, produces a nanostructured TiO_2 surface with mechanical stability, wettability, and bioactivity comparable to or exceeding those achieved with traditional long-duration anodization methods. By significantly reducing processing time without compromising performance, this approach offers a more practical and scalable alternative for industrial application. Its ability to generate a biologically favorable interface suggests strong potential for improving the early stages of osseointegration and, consequently, the long-term success of dental implants.

Author Contribution

B. C. N. S.: Scientific and experimental development of the study, including the execution of the main experimental activities and preparation of the manuscript. P. S.: Supervision of the study; contribution to the development of the methodology; review and revision of the final manuscript; and acquisition of funding. A. B.: Performance of the experimental analyses involving cells at Colorado State University. K. C. P.: Coordination of the laboratory at Colorado State University; supervision of Abhishek Bhattacharjee; contribution to the evaluation and interpretation of the results; and review and revision of the final manuscript. All authors read and approved the final version of the manuscript..

Funding

This work was supported by the National Council for Scientific and Technological Development – CNPq (Grant 311610/2021-8), CAPES Scholarship (Grant 001), and by CAPES/PROEX (Grant 673/2018). The authors also acknowledge Neodent for providing the materials and infrastructure.

Data Availability

The datasets generated during and/or analysed during the current study are available from the corresponding author on reasonable request.

Declarations

Conflict of interest

The authors declare no competing interests.

References

[1] M. Kaur, K. Singh, Review on titanium and titanium based alloys as biomaterials for orthopaedic applications, Materials Science and Engineering: C 102 (2019) 844–862. https://doi.org/10.1016/j.msec.2019.04.064.

[2] I.-S.L. Yeo, Modifications of Dental Implant Surfaces at the Micro- and Nano-Level for Enhanced Osseointegration, Materials 13 (2019) 89. https://doi.org/10.3390/ma13010089.

[3] Q. Wang, P. Zhou, S. Liu, S. Attarilar, R.L.-W. Ma, Y. Zhong, L. Wang, Multi-Scale Surface Treatments of Titanium Implants for Rapid Osseointegration: A Review, Nanomaterials 10 (2020) 1244. https://doi.org/10.3390/nano10061244.

[4] B. Wu, Y. Tang, K. Wang, X. Zhou, L. Xiang, Nanostructured Titanium Implant Surface Facilitating Osseointegration from Protein Adsorption to Osteogenesis: The Example of TiO2 NTAs, International Journal of Nanomedicine 17 (2022) 1865–1879. https://doi.org/10.2147/IJN.S362720.

[5] K. Huo, B. Gao, J. Fu, L. Zhao, P.K. Chu, Fabrication, modification, and biomedical applications of anodized TiO_2 nanotube arrays, RSC Advances 4 (2014) 17300–17324. https://doi.org/10.1039/C4RA01458H.

[6] S. Jafari, B. Mahyad, H. Hashemzadeh, S. Janfaza, T. Gholikhani, L. Tayebi, Biomedical Applications of TiO2 Nanostructures: Recent Advances, International Journal of Nanomedicine 15 (2020) 3447–3470. https://doi.org/10.2147/IJN.S249441.

[7] L. Bai, Y. Zhao, P. Chen, X. Zhang, X. Huang, Z. Du, R. Crawford, X. Yao, B. Tang, R. Hang, Y. Xiao, Targeting Early Healing Phase with Titania Nanotube Arrays on Tunable Diameters to Accelerate Bone Regeneration and Osseointegration, Small 17 (2021). https://doi.org/10.1002/smll.202006287.

[8] Z. Wang, F. Zhao, Y. Zhao, L. Bai, R. Hang, Simultaneously enhanced osteogenesis and angiogenesis via macrophage-derived exosomes upon stimulation with titania nanotubes, Biomaterials Advances 134 (2022) 112708. https://doi.org/10.1016/j.msec.2022.112708.

[9] L. Peng, M.L. Eltgroth, T.J. LaTempa, C.A. Grimes, T.A. Desai, The effect of TiO2 nanotubes on endothelial function and smooth muscle proliferation, Biomaterials 30 (2009) 1268–1272. https://doi.org/10.1016/j.biomaterials.2008.11.012.

[10] E. Beltrán-Partida, B. Valdéz-Salas, A. Moreno-Ulloa, A. Escamilla, M.A. Curiel, R. Rosales-Ibáñez, F. Villarreal, D.M. Bastidas, J.M. Bastidas, Improved in vitro angiogenic behavior on anodized titanium dioxide nanotubes, J. Nanobiotechnology 15 (2017) 10. https://doi.org/10.1186/s12951-017-0247-8.

[11] B. Tao, H. Lan, X. Zhou, C. Lin, X. Qin, M. Wu, Y. Zhang, S. Chen, A. Guo, K. Li, L. Chen, Y. Jiao, W. Yi, Regulation of TiO2 nanotubes on titanium implants to orchestrate osteo/angio-genesis and osteo-immunomodulation for boosted osseointegration, Materials Design 233 (2023) 112268. https://doi.org/10.1016/j.matdes.2023.112268.

[12] D. Regonini, C.R. Bowen, A. Jaroenworaluck, R. Stevens, A review of growth mechanism, structure and crystallinity of anodized TiO2 nanotubes, Materials Science and Engineering: R: Reports 74 (2013) 377–406. https://doi.org/10.1016/j.mser.2013.10.001.

[13] J.M. Macak, H. Tsuchiya, L. Taveira, S. Aldabergerova, P. Schmuki, Smooth anodic TiO2 nanotubes, Angewandte Chemie International Ed. (2005). https://doi.org/10.1002/anie.200502781.

[14] P. Roy, S. Berger, P. Schmuki, TiO2 nanotubes: synthesis and applications., Angewandte Chemie International Ed. (2011). https://doi.org/10.1002/anie.201001374.

[15] K. Indira, U.K. Mudali, T. Nishimura, N. Rajendran, A Review on TiO2 Nanotubes: Influence of Anodization Parameters, Formation Mechanism, Properties, Corrosion Behavior, and Biomedical Applications, Journal of Bio- and Tribo-corrosion 1 (2015) 28. https://doi.org/10.1007/s40735-015-0024-x.

[16] M.L. Puga, J. Venturini, C.S. ten Caten, C.P. Bergmann, Influencing parameters in the electrochemical anodization of TiO2 nanotubes: Systematic review and meta-analysis, Ceramics International 48 (2022) 19513–19526. https://doi.org/10.1016/j.ceramint.2022.04.059.

[17] O. Zakir, A. Ait-Karra, R. Idouhli, M. Khadiri, B. Dikici, A. Aityoub, A. Abouelfida, A. Outzourhit, Effect of anodization time on the morphological, structural, electrochemical, and photocatalytic properties of anodic TiO2 NTs, Journal of Solid State Chemistry 322 (2023) 123939. https://doi.org/10.1016/j.jssc.2023.123939.

[18] R. V Chernozem, M.A. Surmeneva, R.A. Surmenev, Influence of Anodization Time and Voltage on the Parameters of TiO $_2$ Nanotubes, IOP Conference Series: Materials Science and Engineering. 116 (2016) 012025. https://doi.org/10.1088/1757-899X/116/1/012025.

[19] A. Robin, M. Bernardes de Almeida Ribeiro, J. Luiz Rosa, R. Zenhei Nakazato, M. Borges Silva, Formation of TiO2 Nanotube Layer by Anodization of Titanium in Ethylene Glycol-H2O Electrolyte, Journal of Surface Engineered Materials and Advanced Technology 4 (2014) 123–130. https://doi.org/10.4236/jsemat.2014.43016.

[20] T.M. David, P.R. Dev, P. Wilson, P. Sagayaraj, T. Mathews, A critical review on the variations in anodization parameters toward microstructural formation of TiO_2 nanotubes, Electrochemical Science Advances 2 (2022). https://doi.org/10.1002/elsa.202100083.

[21] B. Ribeiro, R. Offoiach, S. Rossetti, E. Salatin, M. Lekka, L. Fedrizzi, On Growth and Morphology of TiO2 Nanotubes on CP-Ti by Anodic Oxidation in Ethylene Glycol Electrolyte: Influence of Electrolyte Aging and Anodization Parameters, Materials 15 (2022) 3338. https://doi.org/10.3390/ma15093338.

[22] Y. Kim, S.K. Mohanty, Electrochemical Synthesis and Morphological Analysis of Titanium Dioxide Nanostructures: Nanotubes, Nanograss, and Nanolace, Advanced Engineering Materials 27 (2025). https://doi.org/10.1002/adem.202402227.

[23] V.A. Maia, F.M. Paschoal, N.A. Braga, TiO2 nanotubes produced by the anodization process under different parameters, Journal of Porous Materials 29 (2022) 1981–1989. https://doi.org/10.1007/s10934-022-01307-0.

[24] S. Sreekantan, Z. Lockman, R. Hazan, M. Tasbihi, L.K. Tong, A.R. Mohamed, Influence of electrolyte pH on TiO2 nanotube formation by Ti anodization, Journal of Alloys and Compounds 485 (2009) 478–483. https://doi.org/10.1016/j.jallcom.2009.05.152.

[25] L. Mohan, C. Dennis, N. Padmapriya, C. Anandan, N. Rajendran, Effect of Electrolyte Temperature and Anodization Time on Formation of TiO2 Nanotubes for Biomedical Applications, Materials Today Communication 23 (2020) 101103. https://doi.org/10.1016/j.mtcomm.2020.101103.

[26] S. Leonardi, V. Russo, A. Li Bassi, F. Di Fonzo, T.M. Murray, H. Efstathiadis, A. Agnoli, J. Kunze-Liebhäuser, TiO2 Nanotubes: Interdependence of Substrate Grain Orientation and Growth Rate, ACS Applied Materials Interfaces 7 (2015) 1662–1668. https://doi.org/10.1021/am507181p.

[27] S. So, K. Lee, P. Schmuki, Ultrafast Growth of Highly Ordered Anodic TiO_2 Nanotubes in Lactic Acid Electrolytes, Journal of the American Chemistry Society 134 (2012) 11316–11318. https://doi.org/10.1021/ja301892g.

[28] M. Benčina, A. Iglič, M. Mozetič, I. Junkar, Crystallized TiO2 Nanosurfaces in Biomedical Applications, Nanomaterials 10 (2020) 1121. https://doi.org/10.3390/nano10061121.

[29] A.C.C.A. Fontes, L. Sopchenski, C.A.H. Laurindo, R.D. Torres, K.C. Popat, P. Soares, Annealing Temperature Effect on Tribocorrosion and Biocompatibility Properties of TiO2 Nanotubes, Journal of Bio- and Tribo-corrosion 6 (2020) 64. https://doi.org/10.1007/s40735-020-00363-w.

[30] M.F. Dias-Netipanyj, L. Sopchenski, T. Gradowski, S. Elifio-Esposito, K.C. Popat, P. Soares, Crystallinity of TiO2 nanotubes and its effects on fibroblast viability, adhesion, and proliferation, Journal of Materials Science: Materials in Medicine 31 (2020) 94. https://doi.org/10.1007/s10856-020-06431-4.

[31] M. Sarraf, A. Razak, R. Crum, C. Gámez, B. Ramirez, N. Kasim, B. Nasiri-Tabrizi, V. Gupta, N. Sukiman, W. Basirun, Adhesion measurement of highly-ordered TiO2 nanotubes on Ti-6Al-4V alloy, Processing and Application of Ceramics 11 (2017) 311–321. https://doi.org/10.2298/PAC1704311S.

[32] M. Manosso, L. Villela, R.D. Torres, C.M. Lepienski, P. Soares, The effect of annealing and surface topography on the mechanical stability of TiO2 nanotubes on titanium implants during insertion test, Journal of the Mechanical Behavior of Biomedical Materials 177 (2026) 107374. https://doi.org/10.1016/j.jmbbm.2026.107374.

[33] F. Rupp, R.A. Gittens, L. Scheideler, A. Marmur, B.D. Boyan, Z. Schwartz, J. Geis-Gerstorfer, A review on the wettability of dental implant surfaces I: Theoretical and experimental aspects, Acta Biomaterialia 10 (2014) 2894–2906. https://doi.org/10.1016/j.actbio.2014.02.040.

[34] R.P. Nogueira, J. Deuzimar Uchoa, F. Hilario, G. de F. Santana-Melo, L.M.R. de Vasconcellos, F.R. Marciano, V. Roche, A. Moreira Jorge Junior, A.O. Lobo, Characterization of Optimized TiO2 Nanotubes Morphology for Medical Implants: Biological Activity and Corrosion Resistance, International Journal of Nanomedicine Volume 16 (2021) 667–682. https://doi.org/10.2147/IJN.S285805.

[35] S. Hosseinpour, F. Tang, F. Wang, R.A. Livingstone, S.J. Schlegel, T. Ohto, M. Bonn, Y. Nagata, E.H.G. Backus, Chemisorbed and Physisorbed Water at the TiO2 Water Interface, The Journal of Physical Chemistry Letters 8 (2017) 2195–2199. https://doi.org/10.1021/acs.jpclett.7b00564.

[36] E.J. Falde, S.T. Yohe, Y.L. Colson, M.W. Grinstaff, Superhydrophobic materials for biomedical applications, Biomaterials 104 (2016) 87–103. https://doi.org/10.1016/j.biomaterials.2016.06.050.

[37] Z. Gong, Y. Hu, F. Gao, L. Quan, T. Liu, T. Gong, C. Pan, Effects of diameters and crystals of titanium dioxide nanotube arrays on blood compatibility and endothelial cell behaviors, Colloids and Surfaces B: Biointerfaces 184 (2019) 110521. https://doi.org/10.1016/j.colsurfb.2019.110521.

[38] E. Balaur, J.M. Macak, L. Taveira, P. Schmuki, Tailoring the wettability of TiO2 nanotube layers, Electrochemistry Communications 7 (2005) 1066–1070. https://doi.org/10.1016/j.elecom.2005.07.014.

[39] D.H. Shin, T. Shokuhfar, C.K. Choi, S.-H. Lee, C. Friedrich, Wettability changes of TiO2 nanotube surfaces, Nanotechnology 22 (2011) 315704. https://doi.org/10.1088/0957-4484/22/31/315704.

[40] R. Wang, N. Sakai, A. Fujishima, T. Watanabe, K. Hashimoto, Studies of Surface Wettability Conversion on TiO $_2$ Single-Crystal Surfaces, The Journal of Physical Chemistry B 103 (1999) 2188–2194. https://doi.org/10.1021/jp983386x.

[41] G. Liu, K. Du, K. Wang, Surface wettability of TiO2 nanotube arrays prepared by electrochemical anodization, Applied Surface Sciences 388 (2016) 313–320. https://doi.org/10.1016/j.apsusc.2016.01.010.

[42] V.B. Damodaran, D. Bhatnagar, V. Leszczak, K.C. Popat, Titania nanostructures: a biomedical perspective, RSC Advances 5 (2015) 37149–37171. https://doi.org/10.1039/C5RA04271B.

[43] T. Li, K. Gulati, N. Wang, Z. Zhang, S. Ivanovski, Understanding and augmenting the stability of therapeutic nanotubes on anodized titanium implants, Materials Science and Engineering: C 88 (2018) 182–195. https://doi.org/10.1016/j.msec.2018.03.007.

[44] C. Dodo, P.M. Senna, A.A. Del Bel Cury, L. Meirelles, Impact of High Insertion Torque on Implant Surface Integrity, Clinical Implant Dentistry and Related Research 27 (2025). https://doi.org/10.1111/cid.70030.

[45] E. Sánchez, E. de Vries, D. Matthews, E. van der Heide, D. Janssen, The effect of coating characteristics on implant-bone interface mechanics, Journal of Biomechanics 163 (2024) 111949. https://doi.org/10.1016/j.jbiomech.2024.111949.